Wakes in inhomogeneous plasmas

Roman Kompaneets,[1,*] Alexei V. Ivlev,[1,†] Vladimir Nosenko,[1,2] and Gregor E. Morfill[1]
[1]*Max-Planck-Institut für extraterrestrische Physik, Giessenbachstr. 1, 85748 Garching, Germany*
[2]*Deutsches Zentrum für Luft- und Raumfahrt, Forschungsgruppe Komplexe Plasmen, Münchener Str. 20, 82234 Weßling, Germany*

(Received 15 January 2014; published 24 April 2014)

The Debye shielding of a charge immersed in a flowing plasma is an old classic problem. It has been given renewed attention in the last two decades in view of experiments with complex plasmas, where charged dust particles are often levitated in a region with strong ion flow. Efforts to describe the shielding of the dust particles in such conditions have been focused on the homogeneous plasma approximation, which ignores the substantial inhomogeneity of the levitation region. We address the role of the plasma inhomogeneity by rigorously calculating the point charge potential in the collisionless Bohm sheath. We demonstrate that the inhomogeneity can dramatically modify the wake, making it nonoscillatory and weaker.

DOI: 10.1103/PhysRevE.89.043108 PACS number(s): 52.27.Lw, 52.40.Kh, 52.30.−q, 52.35.Fp

I. INTRODUCTION

The Debye shielding of a charge immersed in a flowing plasma is an old problem that received considerable attention [1–14], with applications ranging from charging of a spacecraft in the ionosphere [15,16] to spectra of ions moving through solids [17,18]. Various forms of the potential distribution were obtained, depending on model assumptions and parameter values. For instance, in the collisionless case the far-field potential has been shown to generally vary as r^{-3} [4], while in the presence of collisions it can have an r^{-2} dependence [9]. A flowing Maxwellian plasma can generate a series of potential wells downstream of the charge, depending on the flow velocity [11].

The problem has been given renewed attention in the last two decades in view of experiments with complex plasmas, where charged dust particles are often levitated in a region with strong ion flow (see, e.g., Refs. [19–23] for reviews of complex plasma research). Much theoretical effort [24–36] has been made to describe how the charged dust particles are shielded in that region, as the shielding directly determines their mutual electrostatic interaction. The suggested wake models range from those assuming cold flowing ions [24–26] to advanced kinetic models incorporating ion-neutral collisions and the electric field that drives the ion flow and supports the dust particles against gravity [30,34]. A great deal of numerical simulations, based on various assumptions, have been performed [35,37–43]. There have also been measurements of the interaction between the dust particles [44–47], but it is difficult to judge the accuracy of wake models because of experimental uncertainties, limited measurement range of distances, and poorly known parameters in the levitation region (see, e.g., Figs. 1 and 2 of Ref. [34] and Fig. 3 of Ref. [33], where the same measurements were fitted by quite different models by adjusting model parameters).

While theoretical and simulation efforts to describe the wakes generated by the dust particles have been focused on the homogeneous plasma approximation, the levitation region is usually considerably inhomogeneous, as evidenced by measurements of the resonance frequency of vertical oscillations [34,44]. The measured frequency $f_{\mathrm{res}} = \omega_{\mathrm{res}}/(2\pi)$ allows calculating the field inhomogeneity length L_E (via the formula $L_E = g/\omega_{\mathrm{res}}^2$, neglecting the ion drag force [21] and dust charge variations [21]), which turns out to be about the characteristic shielding length in the region (see, e.g., Sec. V B of Ref. [34]).

To the best of our knowledge, there have been no studies of the effect of the inhomogeneity on wake properties. Presumably, this is because the inhomogeneity is challenging to account for: The standard calculation method based on the three-dimensional Fourier transform in space and the dielectric function becomes inapplicable, and the resulting equations entail substantial numerical difficulties.

In this paper, we address the role of the inhomogeneity by rigorously calculating the point-charge potential in the collisionless Bohm sheath [48] (which is one of the best-known "simple" models for an inhomogeneous plasma with ion flow) and comparing the results with the homogeneous approximation. Here, "rigorously" means that we calculate the exact potential, making *no further approximation* in addition to the common linear perturbation approximation. As the collisionless Bohm sheath is a model that has a number of well-known limitations (see Sec. IV), our study is not intended to precisely describe the wake under certain conditions. Our results, however, indicate the essential qualitative changes introduced by the inhomogeneity, which we believe to be the generic features characterizing wakes in inhomogeneous plasma flows.

Note that while our study is concerned with the single-particle wake, dense three-dimensional dust clouds and crystals involve dust-collective effects (i.e., the potential perturbation due to a dust particle is influenced by other dust particles) [49–56]. However, as stated above, our purpose is not to precisely describe the wake under certain conditions, but rather to point out and evaluate the very general and so far unstudied effect of the inhomogeneity. Also, the single-particle wake is the essential reference point to study dust-collective effects, and, as we make clear in Sec. IV A, there are important classes of experiments (e.g., those with dust monolayers, strings, clusters, or pairs) where such effects should be insignificant.

*kompaneets@mpe.mpg.de
†ivlev@mpe.mpg.de

We hope that this paper will be also interesting in that we describe a working method to accurately and effectively calculate the potential due to an extraneous charge in an inhomogeneous plasma (see Appendix A). Implementation of the method is relatively simple, so it may be further utilized for various inhomogeneous plasma environments.

II. MODEL

A. Basic equations

We consider a point nonabsorbing charge q located at $\mathbf{r} = \mathbf{0}$ and immersed in an inhomogeneous plasma consisting of Boltzmann electrons and cold flowing singly ionized ions. A sketch of the problem is shown in Fig. 1. We assume that at $z = -\infty$, the plasma is homogeneous and has a number density n_∞ and an ion flow velocity v_∞ directed in the positive z direction. We set the electric potential at $z = -\infty$ equal to zero and assume that the unperturbed electric potential $\varphi_s(z)$ takes a value $\varphi_0 < 0$ at $z = 0$. (The subscript "s" stands for "sheath"; "unperturbed" refers, here and in the following, to the state in the absence of the charge q.) No wall is included in our model, as we assume that the wall towards which the unperturbed flow is directed [48] is located sufficiently far from the charge; we adopt this assumption in order to investigate the pure effect of the inhomogeneity rather than the combined effect of the inhomogeneity and proximity of the wall. Note that in complex plasma experiments, the particles are usually negatively charged, but in our model the sign of q is unimportant in view of the linear perturbation approximation introduced below.

As illustrated in Fig. 1, in the unperturbed sheath, (1) the ion flow velocity increases with z as ions are accelerated by the electric field, (2) the ion density decreases with z to keep the ion flux constant, and (3) the electron density decreases with z faster than the ion density to ensure a positive net charge density, resulting in the field being directed in the positive z-direction.

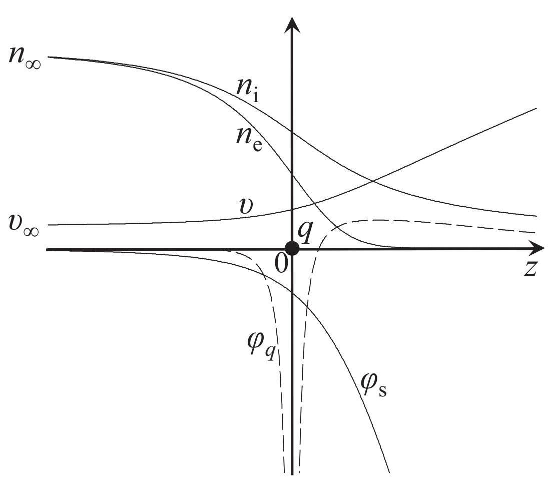

FIG. 1. Sketch of the problem. The solid curves illustrate the unperturbed sheath, showing the electric potential $\varphi_s(z)$, ion number density $n_i(z)$, electron number density $n_e(z)$, and ion flow velocity $v(z)$. The dashed line shows the potential perturbation φ_q (on the z axis) due to the immersed charge $q < 0$.

In the presence of the charge, the system in its steady state is described by the ion continuity equation

$$\nabla \cdot (n_i \mathbf{v}) = 0, \tag{1}$$

ion momentum equation

$$m\,(\mathbf{v} \cdot \nabla)\,\mathbf{v} = -e\nabla\varphi, \tag{2}$$

Boltzmann distribution of electrons

$$n_e = n_\infty \exp\left(\frac{e\varphi}{T_e}\right), \tag{3}$$

and Poisson's equation

$$-\nabla^2\varphi = 4\pi[e(n_i - n_e) + q\delta(\mathbf{r})], \tag{4}$$

where n_i and n_e are the ion and electron number densities, respectively, $\mathbf{v}$ is the ion flow velocity,

$$\varphi = \varphi_s + \varphi_q \tag{5}$$

is the electric potential, with φ_q being the potential perturbation due to the charge (the wake potential), T_e is the electron temperature, m is the ion mass, e is the elementary charge, and $\delta(\mathbf{r})$ is the delta function. The unperturbed system is described by Eqs. (1)–(4) with $q = 0$. We follow the common assumption [48] that the velocity v_∞ is the Bohm velocity,

$$v_\infty = \sqrt{\frac{T_e}{m}}. \tag{6}$$

Below we focus on the wake potential $\varphi_q(\mathbf{r})$. The problem is solved in the linear perturbation approximation (its applicability is discussed in Sec. IV): i.e., we linearize Eqs. (1)–(4) with respect to the perturbations induced by the charge.

B. Solution

We first make the following transformation to rewrite equations in a dimensionless form:

$$\begin{aligned} &\frac{\mathbf{r}}{\lambda_{e\infty}} \to \mathbf{r}, \quad \frac{n_i}{n_\infty} \to n_i, \\ &\frac{\mathbf{v}}{v_\infty} \to \mathbf{v}, \quad \psi = -\frac{e\varphi}{T_e}, \end{aligned} \tag{7}$$

where

$$\lambda_{e\infty} = \sqrt{\frac{T_e}{4\pi n_\infty e^2}} \tag{8}$$

is the electron Debye length at $z = -\infty$ and v_∞ is given by Eq. (6). In these dimensionless notations, Eqs. (1)–(4) take the form

$$\nabla \cdot (n_i \mathbf{v}) = 0, \tag{9}$$

$$(\mathbf{v} \cdot \nabla)\mathbf{v} = \nabla\psi, \tag{10}$$

$$\nabla^2\psi = n_i - \exp(-\psi) + A\delta(\mathbf{r}), \tag{11}$$

where $A = q/(en_\infty\lambda_{e\infty}^3)$. It is convenient to introduce the dimensionless control parameter

$$\psi_0 = -\left.\frac{e\varphi_s}{T_e}\right|_{z=0}, \tag{12}$$

which characterizes the charge location relative to the unperturbed plasma structure.

Calculating the unperturbed variables is nothing but solving the collisionless Bohm sheath model [48]. The unperturbed momentum and continuity equations for ions yield

$$v=\sqrt{1+2\psi},\quad n_{\mathrm{i}}=\frac{1}{\sqrt{1+2\psi}}. \tag{13}$$

We substitute Eq. (13) into the unperturbed Poisson's equation [i.e., Eq. (11) without the last term], multiply it by $d\psi/dz$, and integrate the resulting equation over z from $z=-\infty$ to an arbitrary z using the boundary conditions $\psi|_{z\to-\infty}=0$ and $d\psi/dz|_{z\to-\infty}=0$. This yields a first-order differential equation for $\psi(z)$, whose solution for the boundary condition $\psi|_{z=0}=\psi_0$ is given by

$$z=\frac{1}{\sqrt{2}}\int_{\psi_0}^{\psi}\frac{d\psi'}{\sqrt{\sqrt{1+2\psi'}+\exp(-\psi')-2}}. \tag{14}$$

By using this equation, we calculate $\psi(z)$ numerically, which is further used to calculate $v(z)$ and $n_{\mathrm{i}}(z)$ from Eq. (13). Note that the solid lines illustrating the unperturbed sheath in Fig. 1 are obtained by the exact calculation for $\psi_0=1$ (the range $-10<z<10$ is shown). As seen directly from Eq. (14), choosing a different value of ψ_0 merely results in a constant being added to z, that is, in a shift of the curves along the flow.

To calculate the perturbations, we use the two-dimensional Fourier transform with respect to $\mathbf{r}_\perp$, which is the component of $\mathbf{r}$ perpendicular to the z axis. We linearize Eqs. (9)–(11) with respect to the perturbations and take the Fourier transform of the resulting equations [i.e., we multiply them by $\exp(-i\mathbf{k}_\perp\cdot\mathbf{r}_\perp)$, where $\mathbf{k}_\perp$ is a vector perpendicular to the z axis, and integrate them over $\mathbf{r}_\perp$]. We arrive at

$$\frac{d}{dz}(\hat{n}_{\mathrm{i}}v+n_{\mathrm{i}}\hat{v}_z)+ik_\perp n_{\mathrm{i}}\hat{v}_\perp=0, \tag{15}$$

$$\frac{d(v\hat{v}_z)}{dz}=\frac{d\hat{\psi}}{dz}, \tag{16}$$

$$v\frac{d\hat{v}_\perp}{dz}=ik_\perp\hat{\psi}, \tag{17}$$

$$-k_\perp^2\hat{\psi}+\frac{d^2\hat{\psi}}{dz^2}=\hat{n}_{\mathrm{i}}+\exp(-\psi)\hat{\psi}+A\delta(z), \tag{18}$$

where $\hat{n}_{\mathrm{i}}$, $\hat{v}_z$, $\hat{v}_\perp$, and $\hat{\psi}$ are the Fourier-transformed perturbations (with $\hat{v}_\perp$ being the Fourier transform of the velocity component in the $\mathbf{k}_\perp$ direction), while n_{i}, v, and ψ are the unperturbed quantities given by Eqs. (13) and (14).

Our next steps, described in detail in Appendix A, are (1) to reduce Eqs. (15)–(18) to a single equation for $\hat{\psi}$, (2) to rewrite this equation using the normalization

$$\frac{\varphi_q}{q/\lambda_{\mathrm{e}\infty}}\to\varphi_q, \tag{19}$$

which cancels out the parameter A, (3) to determine the physically correct boundary condition by taking into consideration the Landau damping, (4) to numerically solve the equation using the above boundary condition, and (5) to numerically inverse Fourier transform the result.

C. Reference point: Wake in a homogeneous plasma

To see the effect of the plasma inhomogeneity on $\varphi_q(\mathbf{r})$, we make a comparison with the model in which the unperturbed plasma is homogeneous and has the same electron Debye length, ion density, and ion flow velocity as those in our inhomogeneous model at $z=0$. The potential perturbations $\varphi_q(\mathbf{r})$ obtained in the two models must coincide as $\psi_0\to 0$, which is one of the tests we used to ensure the correctness of our calculations.

In this homogeneous model, the unperturbed potential $\varphi_{\mathrm{s}}(\mathbf{r})$ is obviously zero and the potential perturbation is [4]

$$\varphi_q(\mathbf{r})=\frac{q}{r}+\frac{q}{2\pi^2}\int d\mathbf{k}\,\frac{\exp(i\mathbf{k}\cdot\mathbf{r})}{k^2}\left[\frac{1}{D(\mathbf{k})}-1\right], \tag{20}$$

where

$$D(\mathbf{k})=1+\frac{1}{(\lambda_{\mathrm{e}0}k)^2}-\frac{\omega_{\mathrm{pi}0}^2}{(k_zv_0-i0^+)^2} \tag{21}$$

is the static dielectric function. The relevant electron Debye length and ion plasma frequency are

$$\lambda_{\mathrm{e}0}=\sqrt{\frac{T_{\mathrm{e}}}{4\pi n_{\mathrm{e}0}e^2}},\quad \omega_{\mathrm{pi}0}=\sqrt{\frac{4\pi n_{\mathrm{i}0}e^2}{m}}, \tag{22}$$

respectively, and the subscript "0" denotes the unperturbed quantities taken from our inhomogeneous model at $z=0$. The term $-i0^+$ (where 0^+ is an infinitesimal positive number) represents the Landau damping [33], which is important as it removes the singularity of the integrand in Eq. (20), with the minus sign in $-i0^+$ resulting in the downstream location of the oscillatory wake structure [25]. This makes it obvious that in our inhomogeneous model, we do need to take into consideration the Landau damping, which is step (3) mentioned in Sec. II B. The calculation of the integral (20) is detailed in Appendix B.

III. RESULTS

One may expect the shielding cloud to be considerably affected by the inhomogeneity when the respective spatial scales are comparable. Therefore, before providing our results, we show in Fig. 2 the following unperturbed quantities: the electron Debye length and ion Debye length defined using the ion kinetic energy [33],

$$\lambda_{\mathrm{e}}=\sqrt{\frac{T_{\mathrm{e}}}{4\pi n_{\mathrm{e}}e^2}},\quad \lambda_{\mathrm{i}}=\sqrt{\frac{mv^2}{4\pi n_{\mathrm{i}}e^2}}, \tag{23}$$

as well as the velocity and field inhomogeneity lengths,

$$L_v=v\left(\frac{dv}{dz}\right)^{-1},\quad L_E=E\left(\frac{dE}{dz}\right)^{-1}, \tag{24}$$

where $E=-d\varphi_{\mathrm{s}}/dz$ is the sheath electric field. We see that the inhomogeneity is weak at small ψ and becomes substantial at $\psi\simeq 1$—3, depending on whether L_v or L_E is considered.

Let us start with the potential perturbation in the downstream direction. We note that the integrals over $k_\perp$ determining $\varphi_q(\mathbf{r})$ in both the inhomogeneous and homogeneous models [Eqs. (A14) and (B1), respectively] logarithmically diverge at $k_\perp\to\infty$ on the line $r_\perp=0$, $z>0$ (while outside of that line,

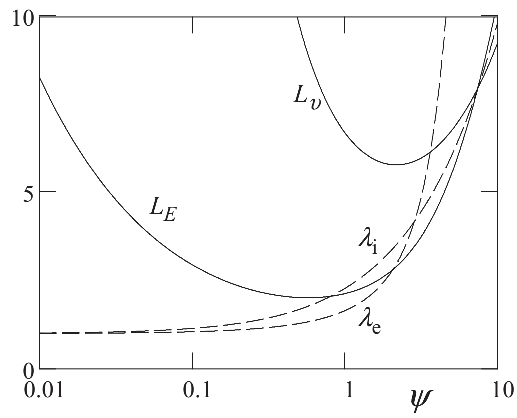

FIG. 2. The velocity and field inhomogeneity lengths, L_v and L_E [Eq. (24)], as well as the electron Debye length λ_e and ion shielding length λ_i [Eq. (23)]. The lengths are normalized by $\lambda_{e\infty}$ and shown as functions of the normalized sheath potential ψ.

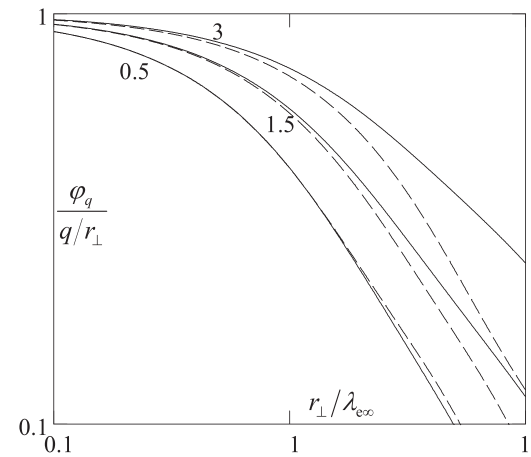

FIG. 4. Potential perturbation in the direction perpendicular to the flow, $\varphi_q(r_\perp; z = 0)$, divided by the Coulomb potential and shown on a log-log graph. The line styles and numbers near the curves bear the same meanings as in Fig. 3.

i.e., for $r_\perp \neq 0$ or $z < 0$, the integrals perfectly converge). The divergence is an artefact of the cold-ion approximation, as explained in Appendix C, and therefore we calculate φ_q on the line $r_\perp = 0$, $z > 0$ by truncating the integration at a certain large $k_\perp$. (In Appendix C, we also discuss the choice of the truncation value.)

Figure 3 shows that the oscillatory wake structure in the flow direction, which is always present in the homogeneous model, disappears in the inhomogeneous model at a rather small ψ_0. The minimum in the potential perturbation is considerably more shallow in the inhomogeneous model. Interestingly, the minimum location is practically unaffected by the inhomogeneity. In the limit $\psi_0 \to 0$, our numerical calculations for both models yield exactly matching oscillatory structures.

Figure 4 shows the potential perturbation in the direction perpendicular to the flow. It is seen to be repulsive (for a charge of the same sign) and not dramatically affected by the inhomogeneity up to $\psi_0 \sim 3$, starting from which the inhomogeneity results in a substantially weaker screening.

Figure 5 shows the absolute value of the derivative $(\partial\varphi_q/\partial z)|_{z=0}$ as a function of $r_\perp$. This quantity, as noted in Sec. IV, is of interest in the context of the mode coupling instability [57–60] observed in two-dimensional plasma crystals. Here we see a remarkably strong effect of the inhomogeneity: The magnitude of the derivative is strongly reduced at $r_\perp \sim \lambda_{e\infty}$ (corresponding to a typical interparticle distance), and the sign changes at a much smaller $r_\perp$ than in the homogeneous case.

Figure 6 shows the contour plots of $\varphi_q(r_\perp, z)$ for (a) the inhomogeneous and (b) homogeneous models, further illustrating the suppression of the oscillatory structure by the inhomogeneity as well as the difference in the derivative $(\partial\varphi_q/\partial z)|_{z=0}$ (compare the angles at which the lines of constant φ_q cross the plane $z = 0$).

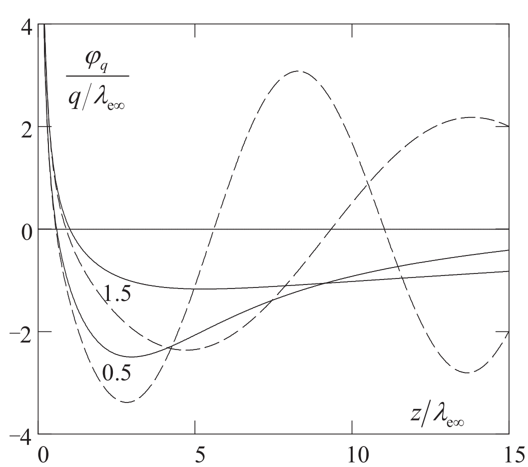

FIG. 3. Potential perturbation in the downstream direction, $\varphi_q(r_\perp = 0; z)$. The solid and dashed lines represent the results of the inhomogeneous and homogeneous models, respectively. The numbers near the curves indicate the values of ψ_0. The graph is obtained by truncating the integration at $k_\perp = 20$ (see text).

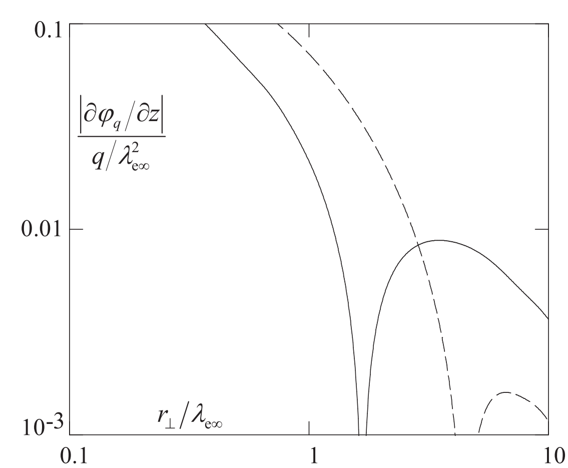

FIG. 5. The derivative $(\partial\varphi_q/\partial z)|_{z=0}$ as a function of $r_\perp$. Shown are the results for $\psi_0 = 1.5$; the line styles bear the same meanings as in Fig. 3.

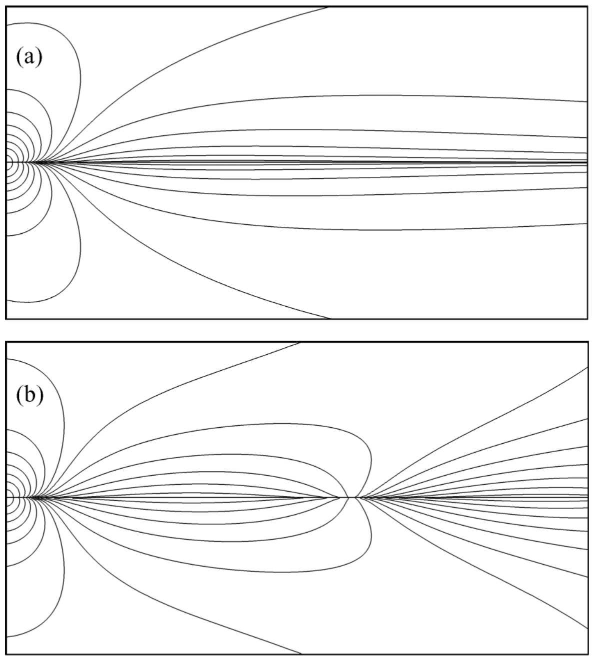

FIG. 6. Potential perturbation $\varphi_q(r_\perp,z)$ for (a) the inhomogeneous and (b) homogeneous models. Shown are lines of constant φ_q for $\psi_0 = 1.5$ (the potential step is not kept constant). The charge is located in the center of the left edge; the flow is directed to the right. In both cases, the dimensions are $15\lambda_{e\infty}$ in the flow direction and $8\lambda_{e\infty}$ in the perpendicular direction. Note that for the cold-ion approximation employed in this paper, in both cases the potential perturbation logarithmically diverges as one approaches the line $r_\perp = 0$, $z > 0$ (also drawn).

IV. DISCUSSION AND CONCLUSIONS

A. Model assumptions

To draw conclusions, let us first discuss the relevance of our model to experiments with complex plasmas.

(1) The sheath is meant to be only a part of the plasma-wall transition layer separating an isotropic plasma from an electrode [48]. It is often unclear whether the dust particles in a given experiment are levitated in the sheath or presheath. An estimate of the electron-to-ion density ratio at the levitation position for a typical experiment [44,45], based on Poisson's equation and the measured resonance frequency of vertical particle oscillations, yields $\simeq 0.85$ [34], suggesting that particles were levitated near the boundary between the sheath and presheath. Sufficiently heavy particles (especially under hypergravity conditions [61]) may be levitated in the sheath. It is noteworthy that while the Bohm sheath model represents a dc regime, most dusty plasma experiments are performed in rf discharges, where electrons respond to the rf field. It is thus clear that the Bohm sheath is not a precise model to describe the levitation region for most experiments. However, to qualitatively understand the effect of the inhomogeneity on the wake, we only need a self-consistent plasma profile that resembles the actual one, and the Bohm sheath model is certainly adequate for such a purpose.

(2) Ions in the levitation region are generally not cold, as they experience collisions on their way through the presheath, forming a velocity distribution with a superthermal width [62–65]. The latter should affect the shielding, as discussed in Sec. IV B in the context of the results of this paper. However, to specifically identify the role of the inhomogeneity, it seems appropriate to start with the simplifying assumption of cold ions. Moreover, measurements of the ion velocity distribution at the electrode show that depending on the pressure and rf power, the characteristic width of the distribution can be considerably smaller than the flow velocity [62], so the cold-ion approximation can be quite reasonable for a certain range of distances from the electrode.

(3) A necessary condition for the model of the collisionless Bohm sheath to be applicable is that the ion-neutral collision length must be much larger than the electron Debye length [66]. For a typical experiment performed at 2.7 Pa [44,45], their ratio is $\simeq 5$ [34]. Hence, the collisionless approximation should be quite reasonable for experiments performed at lower pressures [67–69].

(4) We use the linear perturbation approximation. Nonlinear effects can indeed be substantial for experiments in which the dust particles are levitated in a more or less isotropic region. However, for ion flow velocities of the order of the Bohm velocity, nonlinear effects should be insignificant as the Coulomb radii for ions and electrons, defined as

$$R_\mathrm{i} = \frac{|q|e}{mv^2}, \quad R_\mathrm{e} = \frac{|q|e}{T_\mathrm{e}}, \tag{25}$$

are usually much smaller than the both Debye lengths $\lambda_{\mathrm{i,e}}$ [defined by Eq. (23)]. Nevertheless, nonlinear effects caused by the presence of low-energy ions due to charge-exchange collisions may still affect the shielding to some extent [70].

(5) The assumption of Boltzmann electrons becomes invalid near the wall because of the absorption of electrons on it. However, our model is fully self-consistent as we assume the wall to be located sufficiently far from the charge. Note that in experiments with complex plasmas in rf discharges, the levitation height above the electrode is usually quite large, e.g., an order of magnitude larger than the electron Debye length at the sheath edge [44].

(6) We neglect the influence of the plasma absorption by the dust particle on its shielding. This effect has been given considerable attention in the isotropic case, being attributed primarily to the absorption of ions [71–74]. In the regime of superthermal ion flow, however, the characteristic ion absorption cross section is considerably reduced [19], so the effect of the absorption on the wake should be rather weak (see Ref. [75] for a detailed discussion). To make some estimates, we consider the case $\psi_0 = 0$ for simplicity and use the orbit-motion-limited (OML) cross section [19] for cold-ion flow with the Bohm velocity, $\sigma = \pi a^2(1 + 2z_\mathrm{d})$, where a is the dust particle radius and $z_\mathrm{d} = -qe/(aT_\mathrm{e})$ is the normalized dust charge. We assume that the absorption creates a "shadow" (where the ion density is substantially perturbed by the absorption) of a cross section $\sim\sigma$. The magnitude of the resulting net charge perturbation in that "shadow" within the distance $\lambda_\mathrm{i}(= \lambda_\mathrm{e}$, which is the characteristic shielding length) can be estimated as $\sim e n_\mathrm{i}\sigma\lambda_\mathrm{e} = -q(a/\lambda_\mathrm{e})(2 + z_\mathrm{d}^{-1})/4$, which is usually much less than $-q$ since normally $a/\lambda_\mathrm{e} \sim 10^{-2}$ and $z_\mathrm{d} \sim 3$. Hence, the wake should indeed be not noticeably influenced by the absorption.

(7) The dust-collective effects mentioned in Sec. I are attributed in the literature to the plasma absorption by the dust particles [49–56]. Our model can be extended to include the corresponding term in Eq. (1) for any given dust cloud profile. Note that the literature indicates that this term may become significant only at relatively large distances, e.g., of a few hundreds ion Debye lengths (see, e.g., Fig. 3 of Ref. [51]). Also, such effects operate in large three-dimensional particle clouds and crystals and should be insignificant for monolayers [58,76–78], strings [79,80], clusters [81–83], and pairs [46,84–86], which are also common in experiments.

Now that the relevance of our model has been discussed, let us focus on our findings.

B. Effects of the inhomogeneity

The first effect is the disappearance of the oscillatory wake structure. We note that the presence of these oscillations within the assumption of a homogeneous plasma is model dependent. For instance, the number of the oscillations is infinite for cold ions and Boltzmann electrons, but becomes finite when the ion distribution is a shifted Maxwellian (in which case the far-field potential exhibits a monotonic r^{-3} dependence [4]). In the latter model, the number of the oscillations is determined by the flow-to-thermal velocity ratio as well as the ratio of the temperatures. When the first ratio does not exceed a certain value (of the order of unity), the wake exhibits a single potential well, at least when the electron-to-ion temperature ratio is infinitely large [11]. Hence, a homogeneous model with a realistic ion velocity distribution (whose characteristic width is comparable to the flow velocity [62,63]) may also yield a nonoscillatory wake. The issue is complicated by ion-neutral collisions, the electric field, and that the ion velocity distribution is non-Maxwellian. A model accounting for all these factors can still yield an oscillatory wake, as follows from Eq. (6) of Ref. [34].

The present study suggests that the inhomogeneity tends to suppress the oscillations. Since the inhomogeneity is usually significant in experiments (as noted in Sec. I and discussed in Sec. IV C), one can expect the wake oscillations unlikely to be formed in most experiments, regardless of what homogeneous models predict.

To shed a light on how the oscillations are suppressed by the inhomogeneity, let us focus on the large-z behavior of the Fourier-transformed (over $\mathbf{r}_\perp$) potential perturbation, considering the case $k_\perp = 0$ for simplicity. This behavior is described by

$$\frac{d^2\hat{\varphi}_q}{dz^2} + \frac{n_\mathrm{i}}{v^2}\hat{\varphi}_q = 0, \qquad (26)$$

as follows from Eq. (A3). This has a form of the oscillator equation with a variable frequency. The latter is determined by the unperturbed ion profile [Eqs. (13) and (14)], while the electrons do not contribute, as the Boltzmann factor $\exp(-\psi)$ becomes exponentially small at large z. Obviously, if n_i/v^2 is considered to be constant, Eq. (26) yields an oscillatory structure of $\hat{\varphi}_q$. For the collisionless Bohm sheath, at large z we have $n_\mathrm{i}/v^2 = (2/9)z^{-2}$ (plus the higher-order terms), as follows from Eqs. (13) and (14). For this dependence, the general solution of Eq. (26) becomes nonoscillatory, $\hat{\varphi}_q = C_1 z^{1/3} + C_2 z^{2/3}$, indicating that the inhomogeneity tends to suppress the wake oscillations.

The second effect is that the wake becomes considerably weaker, i.e., φ_q dips to a less negative value (see Fig. 3). This effect is not obvious. On the one hand, in comparison to the homogeneous case, the plasma at $z > 0$ (where the wake is formed) has smaller ion and electron densities and a larger flow velocity and thus may be considered as less capable of considerable "overshielding," so one might indeed expect a weaker wake. But on the other hand, the ion deflection starts long before the ions reach the plane $z = 0$. At this level they already have a transverse velocity, which may be expected to be larger in the inhomogeneous model (because at $z < 0$ the ions are slower and thus more prone to the deflection than in the homogeneous case), so one might expect a larger resulting transverse displacement for $z > 0$ and hence a stronger wake. Our results suggest that the former effect is stronger than the latter one.

Yet another effect is a substantially weaker screening of the Coulomb potential in the perpendicular direction (for a sufficiently strong inhomogeneity). Note that for very large ψ_0, the homogeneous model predicts long-range attraction (for a charge of the same sign) in this direction [33]. In our inhomogeneous model the attraction has not been found, although we did not study the regime of unrealistically large ψ_0 ($\gg 3$). Also note that such attraction was obtained, for a certain set of parameter values, in the study of Ref. [87] including the inhomogeneity along with ion-neutral collisions, ionization, and close proximity of the wall. Since we found the inhomogeneity to weaken the screening in the perpendicular direction, we suggest that the inhomogeneity generally weakens or eliminates the attraction in this direction.

On the other hand, some wake parameters are practically unaffected by the inhomogeneity, for instance, the location of the wake focus (i.e., of the minimum of the wake potential). The same applies to the drag force, which is the electric force exerted by the point charge q on itself through the plasma perturbation. Indeed, in our dimensionless variables, the drag force can be written as

$$F_\mathrm{dr} = \int_0^{R_\mathrm{i}^{-1}} dk_\perp\, k_\perp \left(\frac{1}{2\pi} \left. \frac{d\hat{\varphi}_q}{dz} \right|_{z=0^-} - 1 \right), \qquad (27)$$

which can be obtained from, e.g., Eq. (A14). The well-known logarithmic divergence of the integral for the drag force [11] is avoided here by truncating the integration at $k_\perp = R_\mathrm{i}^{-1}$, where nonlinear effects become significant. (For simplicity we neglect finite-temperature effects, which can come into play before $k_\perp$ reaches R_i^{-1}, see Appendix C. Note that these effects do not remove the divergence of the integral for the drag force [11].) Here R_i is defined by Eq. (25) and normalized by $\lambda_{e\infty}$, the drag force F_dr is normalized by $q^2/\lambda_{e\infty}^2$, and 0^- is an infinitesimal negative number. Since the normalized R_i^{-1} is usually very large (which is the condition to employ the linear perturbation approximation), the drag force is primarily determined by the coefficient of the asymptotic $k_\perp^{-1}$ dependence of the integrand in Eq. (27) (at large $k_\perp$). We have found this coefficient to be *exactly* the same for the inhomogeneous and homogeneous models, which reflects the obvious fact that the plasma inhomogeneity is negligible at small spatial scales ($\sim R_i$).

C. Implications

A natural question arises as to what extent the approximation of a homogeneous plasma is accurate to describe the wakes in experiments with complex plasmas. Obviously, the levitation position and hence the local magnitude of the inhomogeneity depend on the particle size, so let us make some estimates.

We use the collisionless Bohm sheath model in conjunction with the vertical force balance $-qE = Mg$ (where M is the particle mass), neglecting the ion drag for the moment. This results in the following expression for the particle radius $a(\psi_0)$ as a function of the sheath potential at the levitation height:

$$a^2(\psi_0) = \frac{3T_e^2 z_d(\psi_0)}{2\sqrt{2}\pi\rho g e^2 \lambda_{e\infty}} \sqrt{\sqrt{1+2\psi_0} + \exp(-\psi_0) - 2}, \tag{28}$$

where ρ is the particle material mass density and $z_d(\psi_0) = -qe/(aT_e)$ is the normalized dust charge, which we find from the charging equation $I_i = I_e$. We assume the ion and electron fluxes on the particle, $I_{i,e}(\psi_0)$, to be given by the OML theory for cold flowing ions and Maxwellian electrons [19,21], which yields

$$\left[1 + \frac{2z_d(\psi_0)}{1+2\psi_0}\right] \exp\left[z_d(\psi_0) + \psi_0\right] = \sqrt{\frac{8m}{\pi m_e}}, \tag{29}$$

where m_e is the electron mass. Here we used Eqs. (3) and (13) to express the ion and electron densities as well as the flow velocity as functions of ψ_0. Additionally, we need to take into account the stability condition,

$$\frac{d}{dz}\left[z_d[\psi(z)]\frac{d\psi(z)}{dz}\right]\bigg|_{z=0} > 0. \tag{30}$$

By analyzing Eqs. (28)–(30) for typical values $\rho = 1.5\ \mathrm{g/cm^3}$, $\lambda_{e\infty} = 0.5$ mm, $T_e = 2$ eV, and an argon plasma [44,45], we find the largest dust radius for which the levitation is possible to be $a \simeq 6.6\ \mu$m, which corresponds to $\psi_0 \simeq 2.7$. For smaller particles the value of ψ_0 is lower, reaching 0.5 at $a \simeq 3.4\ \mu$m, which is a typical dust radius for experiments. At this point the inhomogeneity still affects the wake considerably (see Fig. 3), so the dust size must be substantially further reduced for the homogeneous approximation to become accurate. Note that much smaller (submicron) particles should rather be levitated in the presheath, where Eqs. (28) and (29) are inappropriate.

To estimate the role of the ion drag, we use the following expression:

$$F_{dr} = \frac{q^2\omega_{pi0}^2}{v_0^2} \ln \Lambda_0, \tag{31}$$

where the prelogarithmic factor is the coefficient of the asymptotic $k_\perp^{-1}$ dependence of the integrand in Eq. (27) at large $k_\perp$ (written in the dimensional variables), the Coulomb logarithm is taken to be

$$\ln \Lambda_0 = \ln\left(\frac{\lambda_{i0}}{R_{i0}}\right), \tag{32}$$

and the subscript "0" is used to explicitly refer to the particle location. By using Eq. (31), we find the ratio of the ion drag to gravity forces to be $\simeq 0.2$ at $\psi_0 = 0.5$. Since this ratio decreases with ψ_0, the ion drag should not considerably affect the vertical force balance unless the particle is rather small.

These simple estimates indicate that for experiments with complex plasmas, homogeneous wake models are accurate only under rather special conditions, e.g., if the dust particles are rather small or levitated by the thermophoresis force [88], gas flow [89], or under microgravity conditions [90–94]. Speaking in terms of the inhomogeneity scale, the velocity inhomogeneity length L_v must be at least an order of magnitude larger than λ_i (the length characterizing the collective ion response) in order for the inhomogeneity to not affect the wake considerably (see Fig. 3 in conjunction with Fig. 2).

By modifying the wakes, the plasma inhomogeneity affects a variety of static and dynamic phenomena. For instance, the inhomogeneity effect on the derivative $\partial\varphi_q/\partial z|_{z=0}$ (see Fig. 5) should influence the development of the mode-coupling instability in two-dimensional plasma crystals [57–60,95]: The growth rate of the instability is proportional to the above derivative [57], so that the critical pressure (at which the instability is suppressed by the gas friction) strongly depends on the inhomogeneity. Furthermore, the weakening of the wake should affect the stability of vertical dust pairs [46,84–86], while the weakening of the screening in the perpendicular direction implies stronger interparticle interactions in two-dimensional plasma crystals.

Yet another implication is that since the inhomogeneity tends to suppress the long-range attraction in the perpendicular direction (for a charge of the same sign), it may be difficult to experimentally realize a molecular-type interaction potential in two-dimensional plasma crystals.

D. Conclusions

We have demonstrated that the plasma inhomogeneity can dramatically modify the wake, making it nonoscillatory and weaker. We expect this to occur in many laboratory experiments with complex plasmas as the inhomogeneity in such experiments is usually quite significant.

ACKNOWLEDGMENTS

The authors thank the anonymous referees for useful comments. The work received funding from the European Research Council under the European Union's Seventh Framework Programme (FP7/2007–2013)/ERC Grant agreement 267499.

APPENDIX A: CALCULATION OF φ_q FROM EQS. (15)–(18)

In this appendix, we explain steps (1)–(5) mentioned in Sec. II B. Concerning step (1), we first express $\hat{v}_z$ and $\hat{v}_\perp$ via $\hat{\psi}$ by using Eqs. (16) and (17) as well as the boundary conditions $\hat{v}_z|_{z=-\infty} = 0$, $\hat{v}_\perp|_{z=-\infty} = 0$, and $\hat{\psi}|_{z=-\infty} = 0$, which yields

$$\hat{v}_z = \frac{\hat{\psi}}{v} \tag{A1}$$

and

$$\hat{v}_\perp = ik_\perp \int_{-\infty}^{z} dz' \, \frac{\hat{\psi}(z')}{v(z')}. \tag{A2}$$

This allows us to express $\hat{n}_\mathrm{i}$ via $\hat{\psi}$, by substituting Eqs. (A1) and (A2) into Eq. (15) and integrating it from $z = -\infty$ to an arbitrary z with the boundary condition $\hat{n}_\mathrm{i}|_{z=-\infty} = 0$. By substituting the result into Eq. (18), we obtain an integro-differential equation for $\hat{\psi}$. By rewriting it in terms of the normalized φ_q [see Eq. (19)], which is step (2), we get

$$\frac{d^2\hat{\varphi}_q}{dz^2} = \left[k_\perp^2 - \frac{n_\mathrm{i}}{v^2} + \exp(-\psi)\right]\hat{\varphi}_q + \frac{k_\perp^2}{v} \int_{-\infty}^{z} dz'\, n_\mathrm{i}(z') \int_{-\infty}^{z'} dz'' \, \frac{\hat{\varphi}_q(z'')}{v(z'')} - 4\pi\delta(z), \tag{A3}$$

where $\hat{\varphi}_q$ is the Fourier transform (with respect to $\mathbf{r}_\perp$) of the potential perturbation normalized as per Eq. (19).

To find the physically correct boundary condition for Eq. (A3), which is step (3), we employ the fact that the physically correct solution $\hat{\varphi}_q(z)$ must vanish at $z \to -\infty$ after correction for the Landau damping. At $z \to -\infty$, Eq. (A3) becomes an equation with constant coefficients, so all its possible asymptotic solutions are linear combinations of $\exp(ik_{z*}z)$. The numbers k_{z*} can be easily found analytically from Eq. (A3) to be two real roots as well as two imaginary roots with opposite signs. The numbers k_{z*} can also be obtained as the roots of the dielectric function (21) with n_{e0} and n_{i0} replaced by n_∞, and v_0 by v_∞:

$$1 + \frac{1}{k_{z*}^2 + k_\perp^2} - \frac{1}{(k_{z*} - i0^+)^2} = 0. \tag{A4}$$

The term $-i0^+$ represents the Landau damping, as stated in Sec. II A. By solving the above equation, we find that the Landau damping results in infinitesimal *positive* imaginary corrections to both "real" roots, meaning that the corresponding solutions grow exponentially as $z \to -\infty$. Excluding these roots as well as the imaginary root with a positive imaginary part, we get only one k_{z*} remaining. This k_{z*} yields the following long-distance behavior:

$$z \to -\infty: \quad \hat{\varphi}_q \propto \exp(\gamma z), \tag{A5}$$

where

$$\gamma = \sqrt{\frac{k_\perp^2}{2} + k_\perp \sqrt{1 + \frac{k_\perp^2}{4}}}. \tag{A6}$$

For the numerical integration, we convert Eq. (A3) into a system of first-order differential equations by introducing the following new variables:

$$\chi = \frac{d\hat{\varphi}_q}{dz}, \quad I_1 = \int_{-\infty}^{z} dz' \, \frac{\hat{\varphi}_q(z')}{v(z')}, \quad I_2 = \int_{-\infty}^{z} dz' \, n_\mathrm{i}(z') I_1(z'). \tag{A7}$$

The resulting system (for $z \neq 0$) is

$$\frac{d\chi}{dz} = \left[k_\perp^2 - \frac{n_\mathrm{i}}{v^2} + \exp(-\psi)\right]\hat{\varphi}_q + \frac{k_\perp^2}{v} I_2, \quad \frac{d\hat{\varphi}_q}{dz} = \chi, \quad \frac{dI_1}{dz} = \frac{\hat{\varphi}_q}{v}, \quad \frac{dI_2}{dz} = n_\mathrm{i} I_1. \tag{A8}$$

The delta-function in Eq. (A3) leads to the following condition:

$$\chi|_{z=0^+} - \chi|_{z=0^-} = -4\pi, \tag{A9}$$

while $\hat{\varphi}_q(z)$, $I_1(z)$, and $I_2(z)$ must be continuous at $z = 0$.

We set the starting point $z = z_-$ of the numerical integration of Eq. (A8) to be a large negative number such that varying the latter does not affect the wake potential in the region of interest. (Similar variation tests are performed for all "internal" parameters of the numerical procedure detailed below.) We use the following boundary conditions at $z = z_-$:

$$z = z_-: \quad \chi = \gamma\hat{\varphi}_q, \quad I_1 = \frac{\hat{\varphi}_q}{\gamma}, \quad I_2 = \frac{\hat{\varphi}_q}{\gamma^2}, \tag{A10}$$

which follow from Eqs. (A5) and (A7). We find $\hat{\varphi}_q(z_-)$ by requiring that the numerical integration of the system (A8) with the boundary conditions (A10) yields $\hat{\varphi}_q = 0$ at the end point $z = z_+$. The latter is a large positive number such that varying it does not affect the wake potential in the region of interest (similar to the starting point z_-). Note that the condition $\hat{\varphi}_q(z_+) = 0$ implies a conducting wall at $z = z_+$. We use the bisection method to find $\hat{\varphi}_q(z_-)$, initially choosing two guess values resulting in opposite signs of $\hat{\varphi}_q$ at $z = z_+$. To integrate Eq. (A8), we simply use Euler's method with a sufficiently small fixed integration step.

A difficulty arises at this point: It turns out that unless $k_\perp$ is not small enough, even a tiny relative difference between the "upper" and "lower" values of $\hat{\varphi}_q(z_-)$ obtained by the above bisection method results in a strong deviation between the corresponding "upper" and "lower" curves $\hat{\varphi}_q(z)$ at positive z. Clearly, this does not hinder calculation of $\hat{\varphi}_q(z_-)$, but the problem is to achieve the sufficient accuracy for $\hat{\varphi}_q(z)$.

To resolve the difficulty, we employ the following method. We stop the bisection procedure as soon as the difference between the "upper" and "lower" values of $\hat{\varphi}_q(z_-)$ becomes smaller than a certain threshold Δ_min, and then we integrate the system (A8) to the point of the z axis at which the deviation between the corresponding "upper" and "lower" curves $\hat{\varphi}_q(z)$ exceeds another threshold $\Delta_\mathrm{max}(>\Delta_\mathrm{min})$. The next step is to reduce the uncertainty of $\hat{\varphi}_q$ at this point to Δ_min. To do this, we first integrate Eq. (A8) from this point using the middle values of $\hat{\varphi}_q$, χ, I_1, and I_2 at this point as the initial conditions. Depending on the resulting sign of $\hat{\varphi}_q(z_+)$, the above middle values become the new "upper" or "lower" values, and this bisection procedure continues until the uncertainty in $\hat{\varphi}_q$ at the above point is reduced to Δ_min. Then we find the next point of the z axis at which the deviation between the "upper" and "lower" $\hat{\varphi}_q$ curves again exceeds Δ_max. The cycle continues until the difference between the "upper" and "lower" $\hat{\varphi}_q$ at $z = z_+$ does not exceed Δ_max. Obviously, the numbers $\Delta_\mathrm{min,max}$ are chosen to be sufficiently small. Interestingly, the computation time turns out to be quite insensitive to Δ_min for a fixed Δ_max.

The wake potential is the inverse Fourier transform (over $\mathbf{k}_\perp$) of the resulting solution $\hat{\varphi}_q(z,k_\perp)$:

$$\varphi_q(\mathbf{r}) = \frac{1}{(2\pi)^2}\int d\mathbf{k}_\perp\, \hat{\varphi}_q(z,k_\perp)\exp(i\mathbf{k}_\perp\cdot\mathbf{r}_\perp). \quad \text{(A11)}$$

We rewrite the integral in the polar coordinates $k_\perp$, α and integrate analytically over the angle α, which yields

$$\varphi_q(\mathbf{r}) = \frac{1}{2\pi}\int_0^\infty dk_\perp\, k_\perp \hat{\varphi}_q(z,k_\perp) J_0(k_\perp r_\perp), \quad \text{(A12)}$$

where J_0 is the zero-order Bessel function of the first kind. The integral in Eq. (A12) diverges on the line $r_\perp = 0$, $z \geqslant 0$. Outside of that line, it converges, but for sufficiently small $|z|$ the convergence is quite slow at large $k_\perp$, where the numerical integration of the system (A8) using the method described above turns out to be particularly time consuming. To circumvent the difficulty, we separate the unscreened Coulomb potential from the total potential perturbation. The Fourier transform (over $\mathbf{r}_\perp$) of the Coulomb potential $\varphi_C = 1/r$ is

$$\hat{\varphi}_C = \int d\mathbf{r}_\perp \frac{\exp(-i\mathbf{k}_\perp\cdot\mathbf{r}_\perp)}{\sqrt{r_\perp^2+z^2}} = \frac{2\pi}{k_\perp}\exp(-k_\perp|z|). \quad \text{(A13)}$$

The potential perturbation φ_q can then be written as the sum of φ_C and the inverse Fourier transform of $\hat{\varphi}_q - \hat{\varphi}_C$:

$$\varphi_q(\mathbf{r}) = \frac{1}{r} + \frac{1}{2\pi}\int_0^\infty dk_\perp\, k_\perp J_0(k_\perp r_\perp) \times \left[\hat{\varphi}_q(z,k_\perp) - \frac{2\pi}{k_\perp}\exp(-k_\perp|z|)\right]. \quad \text{(A14)}$$

Outside of the line $r_\perp = 0$, $z > 0$, the resulting integral converges rather fast even for small $|z|$. We calculate it using Boole's rule with a sufficiently small fixed step. Note that for $z > 0$, the integrand is $\propto J_0(k_\perp r_\perp)k_\perp^{-1}$ at large $k_\perp$. As soon as it reaches this asymptotic dependence, we use the corresponding proportionality coefficient to calculate the integrand for larger $k_\perp$ without solving Eq. (A8).

APPENDIX B: CALCULATION OF φ_q FROM EQ. (20)

To calculate the potential perturbation φ_q in the homogeneous approximation, we first rewrite the integral (20) in the cylindrical coordinates k_z, $k_\perp$, α and analytically integrate over the angle α. This yields

$$\varphi_q(\mathbf{r}) = \frac{1}{r} + \frac{1}{\pi}\int_0^\infty dk_\perp\, k_\perp \int_{-\infty}^\infty dk_z\, J_0(k_\perp r_\perp)\exp(ik_z z) \times \left[\frac{1}{k_\perp^2 + k_z^2 + n_{e0} - \frac{(k_\perp^2+k_z^2)n_{i0}}{(k_z v_0 - i0^+)^2}} - \frac{1}{k_\perp^2+k_z^2}\right], \quad \text{(B1)}$$

where the distances are normalized by $\lambda_{e\infty}$, n_{i0} and n_{e0} by n_∞, v_0 by v_∞, and φ_q as per Eq. (19).

The next step is to analytically perform the integration over k_z in Eq. (B1) by using the residue theorem and Jordan's lemma. The poles of the integrand include two real numbers unless the $-i0^+$ term is accounted for. The latter results in infinitesimal *positive* imaginary corrections to both of them. We get for $z > 0$:

$$\varphi_q(\mathbf{r}) = \frac{1}{r} + \int_0^\infty dk_\perp\, J_0(k_\perp r_\perp) \times \left[\sum_{j=1}^3 S_j(k_\perp,z) - \exp(-k_\perp z)\right], \quad \text{(B2)}$$

where

$$\begin{aligned} S_j(k_\perp,z) &= \frac{ik_\perp \exp[ik_{zj}(k_\perp)z]}{k_{zj}(k_\perp) + \frac{n_{i0}k_\perp^2}{k_{zj}^3(k_\perp)v_0^2}}, \\ k_{z1,z2}(k_\perp) &= \pm\sqrt{B(k_\perp)+C(k_\perp)}, \\ k_{z3}(k_\perp) &= i\sqrt{-B(k_\perp)+C(k_\perp)}, \\ B(k_\perp) &= \frac{n_{i0}}{2v_0^2} - \frac{k_\perp^2+n_{e0}}{2}, \\ C(k_\perp) &= \sqrt{B^2(k_\perp) + \frac{n_{i0}k_\perp^2}{v_0^2}}. \end{aligned} \quad \text{(B3)}$$

We numerically calculate the integral (B2) by using Boole's rule with a fixed integration step.

APPENDIX C: ON THE CHOICE OF THE MAXIMUM $k_\perp$ FOR $r_\perp = 0$, $z > 0$

For any point on the line $r_\perp = 0$, $z > 0$, the integrals over $k_\perp$ in Eqs. (A14) and (B1) diverge at $k_\perp \to \infty$ as $\int dk_\perp\, k_\perp^{-1}$. Outside of that line these integrals converge, behaving at large $k_\perp$ as $\int dk_\perp\, k_\perp^{-1} J_0(k_\perp r_\perp)$ for $z > 0$.

The divergence is due to the cold-ion approximation as it is absent for a shifted Maxwellian ion distribution and Boltzmann electrons [27]. Let us consider the latter case, assuming a homogeneous plasma with ion and electron number densities n_∞, the Bohm ion flow velocity, and a finite ion temperature T_i. Then the potential perturbation for $r_\perp = 0$ is (in our dimensionless notations)

$$\varphi_q(z) = \frac{1}{|z|} + \int_0^\infty dk_\perp\, F(z,k_\perp), \quad \text{(C1)}$$

where the integrand is

$$F(z,k_\perp) = -\exp(-k_\perp|z|) + \frac{k_\perp}{\pi}\int_{-\infty}^\infty dk_z\, \exp(ik_z z) \times \left\{k_z^2 + k_\perp^2 + 1 + \tau^{-1}[1 - \xi Z(-\xi)]\right\}^{-1}, \quad \text{(C2)}$$

$$\xi(k_z,k_\perp) = \frac{k_z}{\sqrt{2\tau(k_z^2+k_\perp^2)}}, \quad \text{(C3)}$$

$Z(x) = 2i\exp(-x^2)\int_{-\infty}^{ix}\exp(-\eta^2)\,d\eta$ is the plasma dispersion function, and $\tau = T_i/T_e$ [4,27]. For $\tau = 5\times10^{-3}$ (corresponding to $T_e = 5$ eV, $T_i = 300$ K) and $z \sim 1$ we find that $F(z,k_\perp)$ starts substantially deviating (by a factor of 2) from the integrand of Eq. (B2) (for $\psi_0 = 0$) at $k_\perp \sim 20$, which is the truncation value we used to plot Fig. 3.

Note that the finite ion temperature affects the period of the spatial potential oscillations downstream of the charge, so the difference in the oscillation phase accumulates with z. Thus, φ_q calculated at $z \gg 1$ for zero and finite ion temperatures may be quite different despite little change of the oscillatory structure. For this reason, we only used $z \sim 1$ to estimate the proper truncation value.

As pointed out in Sec. IV B, nonlinear effects become significant at $k_\perp \sim R_\mathrm{i}^{-1}$, where R_i is defined by Eq. (25) and normalized by $\lambda_{\mathrm{e}\infty}$. To estimate R_i^{-1}, we consider the case $\psi_0 = 0$ and use typical values $\lambda_{\mathrm{e}\infty} = 0.5$ mm, $T_\mathrm{e} = 5$ eV, $a = 3\ \mu$m as well as the charging equation (29), which yields $R_\mathrm{i}^{-1} \simeq 40$. Thus, for the above parameter values, nonlinear effects should become significant at $k_\perp$ larger than (or at least of the same order as) the truncation value for finite-temperature effects.

We have numerically confirmed that for both the inhomogeneous and homogeneous models, the chosen truncation value of 20 is large enough for $\varphi_q(r_\perp = 0; z > 0)$ to reach its asymptotic logarithmic dependence on the truncation value (except for very small z). To illustrate this, we note that Eq. (B2) yields the following logarithmic dependence in the limit of large truncation value k_tr:

$$r_\perp = 0, z > 0: \quad \varphi_q = -2\frac{\sqrt{n_{\mathrm{i}0}}}{v_0}\sin\left(z\frac{\sqrt{n_{\mathrm{i}0}}}{v_0}\right)\ln k_\mathrm{tr}. \tag{C4}$$

For $k_\mathrm{tr} = 20$, this analytic expression quite accurately describes $\varphi_q(z)$ shown in Fig. 3 for the homogeneous case (except for very small z); for instance, the difference in the value of φ_q at the first minimum is $\simeq 5$ % for $\psi_0 = 0.5$ and $\simeq 10$ % for $\psi_0 = 1.5$.

We have also numerically confirmed that our inhomogeneous and homogeneous models yield different prelogarithmic coefficients characterizing the logarithmic dependence of $\varphi_q(r_\perp = 0; z > 0)$ on k_tr at large k_tr. Thus, to see the effect of the inhomogeneity, it is sufficient to choose k_tr to be large enough for $\varphi_q(r_\perp = 0; z > 0)$ to reach its asymptotic logarithmic dependence on k_tr.

[1] J. Neufeld and R. H. Ritchie, Phys. Rev. **98**, 1632 (1955).
[2] I. Oppenheim and N. G. van Kampen, Phys. Fluids **7**, 813 (1964).
[3] G. Joyce and D. Montgomery, Phys. Fluids **10**, 2017 (1967).
[4] D. Montgomery, G. Joyce, and R. Sugihara, Plasma Phys. **10**, 681 (1968).
[5] G. Cooper, Phys. Fluids **12**, 2707 (1969).
[6] J. R. Sanmartin and S. H. Lam, Phys. Fluids **14**, 62 (1971).
[7] E. W. Laing, A. Lamont, and P. Fielding, J. Plasma Phys. **5**, 441 (1971).
[8] P. Chenevier, J. M. Dolique, and H. Peres, J. Plasma Phys. **10**, 185 (1973).
[9] L. Stenflo, M. Y. Yu, and P. K. Shukla, Phys. Fluids **16**, 450 (1973).
[10] C. Wang, G. Joyce, and D. R. Nicholson, J. Plasma Phys. **25**, 225 (1981).
[11] T. Peter, J. Plasma Phys. **44**, 269 (1990).
[12] E. E. Trofimovich and V. P. Krainov, Zh. Eksp. Teor. Fiz. **104**, 3971 (1993) [JETP **77**, 910 (1993)].
[13] D. Else, R. Kompaneets, and S. V. Vladimirov, Phys. Rev. E **82**, 026410 (2010).
[14] R. L. Dewar and D. Leykam, Plasma Phys. Control. Fusion **54**, 014002 (2012).
[15] Y. L. Al'pert, L. Gurevich, A. Quarteroni, and L. P. Pitaevskii, *Space Physics with Artificial Satellites* (Consultants Bureau, New York, 1965).
[16] J. C. Taylor, Planet. Space Sci. **15**, 155 (1967).
[17] F. Bell, H.-D. Betz, H. Panke, and W. Stehling, J. Phys. B **9**, L443 (1976).
[18] D. H. Jakubassa, J. Phys. C: Solid State Phys. **10**, 4491 (1977).
[19] V. E. Fortov, A. V. Ivlev, S. A. Khrapak, A. G. Khrapak, and G. E. Morfill, Phys. Rep. **421**, 1 (2005).
[20] O. Ishihara, J. Phys. D: Appl. Phys. **40**, 121 (2007).
[21] G. E. Morfill and A. V. Ivlev, Rev. Mod. Phys. **81**, 1353 (2009).
[22] P. K. Shukla and B. Eliasson, Rev. Mod. Phys. **81**, 25 (2009).
[23] M. Bonitz, C. Henning, and D. Block, Rept. Prog. Phys. **73**, 066501 (2010).
[24] S. V. Vladimirov and M. Nambu, Phys. Rev. E **52**, R2172 (1995).
[25] S. V. Vladimirov and O. Ishihara, Phys. Plasmas **3**, 444 (1996).
[26] O. Ishihara and S. V. Vladimirov, Phys. Plasmas **4**, 69 (1997).
[27] M. Lampe, G. Joyce, G. Ganguli, and V. Gavrishchaka, Phys. Plasmas **7**, 3851 (2000).
[28] S. Benkadda, V. N. Tsytovich, and S. V. Vladimirov, Phys. Rev. E **60**, 4708 (1999).
[29] G. Lapenta, Phys. Rev. E **62**, 1175 (2000).
[30] V. A. Schweigert, Phys. Rep. **27**, 997 (2001); A. V. Ivlev, S. K. Zhdanov, S. A. Khrapak, and G. E. Morfill, Phys. Rev. E **71**, 016405 (2005).
[31] L.-J. Hou, Y.-N. Wang, and Z. L. Mišković, Phys. Rev. E **64**, 046406 (2001).
[32] M. Lampe, G. Joyce, G. Ganguli, and V. Gavrishchaka, Phys. Scr. **T89**, 106 (2001).
[33] R. Kompaneets, S. V. Vladimirov, A. V. Ivlev, and G. Morfill, New J. Phys. **10**, 063018 (2008).
[34] R. Kompaneets, U. Konopka, A. V. Ivlev, V. Tsytovich, and G. Morfill, Phys. Plasmas **14**, 052108 (2007).
[35] P. Ludwig, W. J. Miloch, H. Kählert, and M. Bonitz, New J. Phys. **14**, 053016 (2012).
[36] D. Block, J. Carstensen, P. Ludwig, W. J. Miloch, F. Greiner, A. Piel, M. Bonitz, and A. Melzer, Contrib. Plasma Phys. **52**, 804 (2012).
[37] G. Lapenta, Phys. Plasmas **6**, 1442 (1999).
[38] G. Lapenta, Phys. Rev. E **66**, 026409 (2002).
[39] W. J. Miloch, S. V. Vladimirov, H. L. Pécseli, and J. Trulsen, Phys. Rev. E **77**, 065401 (2008).
[40] W. J. Miloch, J. Trulsen, and H. L. Pécseli, Phys. Rev. E **77**, 056408 (2008).
[41] W. J. Miloch, Plasma Phys. Controlled Fusion **52**, 124004 (2010).
[42] C. T. N. Willis, J. E. Allen, M. Coppins, and M. Bacharis, Phys. Rev. E **84**, 046410 (2011).
[43] I. H. Hutchinson, Phys. Rev. E **85**, 066409 (2012).
[44] U. Konopka, Ph.D. thesis, Ruhr-Universität-Bochum, 2000.

[45] U. Konopka, G. E. Morfill, and L. Ratke, Phys. Rev. Lett. **84**, 891 (2000).
[46] G. A. Hebner, M. E. Riley, and B. M. Marder, Phys. Rev. E **68**, 016403 (2003).
[47] J. Carstensen, F. Greiner, and A. Piel, Phys. Rev. Lett. **109**, 135001 (2012).
[48] K.-U. Riemann, J. Phys. D: Appl. Phys. **24**, 493 (1991).
[49] V. N. Tsytovich and G. E. Morfill, Plasma Phys. Rep. **28**, 171 (2002).
[50] R. Kompaneetz and V. Tsytovich, Contrib. Plasma Phys. **45**, 130 (2005).
[51] S. Ratynskaia, U. de Angelis, S. Khrapak, B. Klumov, and G. E. Morfill, Phys. Plasmas **13**, 104508 (2006).
[52] C. Castaldo, U. de Angelis, and V. N. Tsytovich, Phys. Rev. Lett. **96**, 075004 (2006).
[53] V. Tsytovich, R. Kompaneets, U. de Angelis, and C. Castaldo, Contrib. Plasma Phys. **46**, 280 (2006).
[54] M. Chaudhuri, R. Kompaneets, and G. E. Morfill, Phys. Plasmas **17**, 063705 (2010).
[55] U. de Angelis, P. Tolias, and S. Ratynskaia, Phys. Plasmas **19**, 073701 (2012).
[56] P. Tolias and S. Ratynskaia, Phys. Plasmas **20**, 023702 (2013).
[57] A. V. Ivlev and G. Morfill, Phys. Rev. E **63**, 016409 (2000).
[58] L. Couëdel, V. Nosenko, A. V. Ivlev, S. K. Zhdanov, H. M. Thomas, and G. E. Morfill, Phys. Rev. Lett. **104**, 195001 (2010).
[59] L. Couëdel, S. K. Zhdanov, A. V. Ivlev, V. Nosenko, H. M. Thomas, and G. E. Morfill, Phys. Plasmas **18**, 083707 (2011).
[60] T. B. Röcker, A. V. Ivlev, R. Kompaneets, and G. E. Morfill, Phys. Plasmas **19**, 033708 (2012).
[61] J. Beckers, T. Ockenga, M. Wolter, W. W. Stoffels, J. van Dijk, H. Kersten, and G. M. W. Kroesen, Phys. Rev. Lett. **106**, 115002 (2011).
[62] M. Zeuner and J. Meichsner, Vacuum **46**, 151 (1995).
[63] R. Kompaneets, A. V. Ivlev, S. V. Vladimirov, and G. E. Morfill, Phys. Rev. E **85**, 026412 (2012).
[64] M. Lampe, T. B. Röcker, G. Joyce, S. K. Zhdanov, A. V. Ivlev, and G. E. Morfill, Phys. Plasmas **19**, 113703 (2012).
[65] R. Kompaneets, Y. O. Tyshetskiy, and S. V. Vladimirov, Phys. Plasmas **20**, 042108 (2013).
[66] K.-U. Riemann, J. Phys. D: Appl. Phys. **36**, 2811 (2003).
[67] V. Nosenko, A. V. Ivlev, S. K. Zhdanov, M. Fink, and G. E. Morfill, Phys. Plasmas **16**, 083708 (2009).
[68] L. Couëdel, V. Nosenko, S. K. Zhdanov, A. V. Ivlev, H. M. Thomas, and G. E. Morfill, Phys. Rev. Lett. **103**, 215001 (2009).
[69] S. Iwashita, E. Schüngel, J. Schulze, P. Hartmann, Z. Donkó, G. Uchida, K. Koga, M. Shiratani, and U. Czarnetzki, J. Phys. D: Appl. Phys. **46**, 245202 (2013).
[70] I. H. Hutchinson and C. B. Haakonsen, Phys. Plasmas **20**, 083701 (2013).
[71] S. A. Khrapak, B. A. Klumov, and G. E. Morfill, Phys. Rev. Lett. **100**, 225003 (2008).
[72] S. Khrapak and G. Morfill, Contrib. Plasma Phys. **49**, 148 (2009).
[73] M. Chaudhuri, S. A. Khrapak, R. Kompaneets, and G. E. Morfill, IEEE Trans. Plasma Sci. **38**, 818 (2010).
[74] M. Chaudhuri, A. V. Ivlev, S. A. Khrapak, H. M. Thomas, and G. E. Morfill, Soft Matter **7**, 1287 (2011).
[75] Y. Tyshetskiy and S. V. Vladimirov, Phys. Plasmas **17**, 103701 (2010).
[76] A. V. Ivlev, U. Konopka, G. Morfill, and G. Joyce, Phys. Rev. E **68**, 026405 (2003).
[77] S. Ratynskaia, K. Rypdal, C. Knapek, S. Khrapak, A. V. Milovanov, A. Ivlev, J. J. Rasmussen, and G. E. Morfill, Phys. Rev. Lett. **96**, 105010 (2006).
[78] C. A. Knapek, D. Samsonov, S. Zhdanov, U. Konopka, and G. E. Morfill, Phys. Rev. Lett. **98**, 015004 (2007).
[79] A. Homann, A. Melzer, S. Peters, and A. Piel, Phys. Rev. E **56**, 7138 (1997).
[80] T. Misawa, N. Ohno, K. Asano, M. Sawai, S. Takamura, and P. K. Kaw, Phys. Rev. Lett. **86**, 1219 (2001).
[81] A. Melzer, M. Klindworth, and A. Piel, Phys. Rev. Lett. **87**, 115002 (2001).
[82] T. E. Sheridan and W. L. Theisen, Phys. Plasmas **13**, 062110 (2006).
[83] K. Qiao, J. Kong, E. V. Oeveren, L. S. Matthews, and T. W. Hyde, Phys. Rev. E **88**, 043103 (2013).
[84] V. Steinberg, R. Sütterlin, A. V. Ivlev, and G. Morfill, Phys. Rev. Lett. **86**, 4540 (2001).
[85] J. Carstensen, F. Greiner, and A. Piel, Phys. Plasmas **17**, 083703 (2010).
[86] J. Carstensen, F. Greiner, D. Block, J. Schablinski, W. J. Miloch, and A. Piel, Phys. Plasmas **19**, 033702 (2012).
[87] A. M. Ignatov, Plasma Phys. Rep. **30**, 865 (2004).
[88] H. Rothermel, T. Hagl, G. E. Morfill, M. H. Thoma, and H. M. Thomas, Phys. Rev. Lett. **89**, 175001 (2002).
[89] M. A. Fink, S. K. Zhdanov, M. H. Thoma, H. Höfner, and G. E. Morfill, Phys. Rev. E **86**, 065401 (2012).
[90] A. V. Ivlev, G. E. Morfill, H. M. Thomas, C. Räth, G. Joyce, P. Huber, R. Kompaneets, V. E. Fortov, A. M. Lipaev, V. I. Molotkov *et al.*, Phys. Rev. Lett. **100**, 095003 (2008).
[91] S. A. Khrapak, B. A. Klumov, P. Huber, V. I. Molotkov, A. M. Lipaev, V. N. Naumkin, A. V. Ivlev, H. M. Thomas, M. Schwabe, G. E. Morfill *et al.*, Phys. Rev. E **85**, 066407 (2012).
[92] M. Y. Pustylnik, M. H. Thoma, G. E. Morfill, R. Grimm, and C. Hock, J. Plasma Phys. **78**, 289 (2012).
[93] J. Beckers, D. J. M. Trienekens, and G. M. W. Kroesen, Phys. Rev. E **88**, 055101 (2013).
[94] S. A. Khrapak, M. H. Thoma, M. Chaudhuri, G. E. Morfill, A. V. Zobnin, A. D. Usachev, O. F. Petrov, and V. E. Fortov, Phys. Rev. E **87**, 063109 (2013).
[95] R. Kompaneets, A. V. Ivlev, V. Tsytovich, and G. Morfill, Phys. Plasmas **12**, 062107 (2005).